

Generation of Ultra-Low Power Phononic Combs

Maxim Goryachev,^{1, a)} Serge Galliou,² and Michael E. Tobar¹

¹⁾ARC Centre of Excellence for Engineered Quantum Systems, University of Western Australia, 35 Stirling Highway, Crawley WA 6009, Australia

²⁾FEMTO-ST Institute, Univ. Bourgogne Franche-Comté, CNRS, ENSMM, 26 Rue de l'Épitahe 25000 Besançon, France

(Dated: 14 April 2020)

We demonstrate excitation of phononic frequency combs in a Bulk Acoustic Wave system at a temperature of 20mK using a single tone low power signal source. The observed ultra low power threshold is due to a combination of very high quality factor of 4.2×10^8 and relatively strong nonlinear effects. The observed repetition rate of the comb varies from 0.7 to 2Hz and spans over tens of Hertz. The demonstrated system is fully excited via piezoelectricity and does not require mode spectra engineering and external optical or microwave signals. It is shown that the comb profile significantly depends on geometry of excitation and detection electrodes. Observed strong Duffing nonlinearity below the generation threshold suggests that the system is a phononic analogue to Kerr frequency combs excited in monolithic optical microresonators. The ultra-low power regime opens a way of integrating this phononic system with quantum hybrid systems such as impurity defects and superconducting qubits.

I. INTRODUCTION

Photonic frequency comb generators are an important tool used for many scientific applications allowing to couple distant parts of frequency spectrum¹. Amongst others, these important applications include ultra stable clocks and frequency metrology²⁻⁴ and spectroscopy^{5,6}. All of these system are photonic mostly utilising a carrier signal at an optical frequency and RF or microwave repetition rates. The most popular ways to generate such combs include mode-locked lasers⁷, (four)-wave mixing/Kerr nonlinearity⁸⁻¹¹ or other physical sources of nonlinearities¹². Despite the fact that phononic systems also play an important role in metrology and spectroscopy, demonstration of phononic or acoustic wave combs has been sporadic¹³. Moreover, their complexity, requirements to design a certain mode structure, very high threshold powers¹⁴ and requirement for extra laser sources¹⁵ make these systems inapplicable for many low energy applications. In these applications Bulk Acoustic Wave (BAW) devices found very extensive use, e.g. frequency metrology¹⁶, quantum hybrid systems¹⁷⁻¹⁹ and fundamental physics tests²⁰⁻²³. Additionally both bulk and surface acoustic wave devices are utilised for spectroscopy²⁴, detection and sensors²⁵⁻²⁷. Recently nonlinear dynamics of mechanical systems including comb generation has also become a subject of theoretical research²⁸. All these areas could benefit from designing devices with frequency comb functionality.

II. EXPERIMENTAL SETUP

To excite frequency combs at low power levels, one needs a system with low losses and strong nonlinear

effects. For these reasons, in this work, we employ a phonon trapping²⁹ SC (Stress Compensated) cut³⁰ quartz BAW cavity³¹ operating at 20mK. The device is an SC-cut plano-convex shaped plate of 1mm thickness, 23mm diameter and 300mm radius of curvature. Quartz BAW cavities have demonstrated extremely high values of Quality factors at cryogenic temperatures reaching the level of $8 \times 10^{9,20,31}$. At the same time these devices are able to demonstrate a significant levels of nonlinearities. Traditionally nonlinearities in mechanical system are associated with a Duffing nonlinearity that is a consequence of lattice anharmonicity, i.e. a nonlinear term in Hook's law. This type of nonlinearity has been extensively studied for many types of mechanical systems³²⁻³⁴. Other sources of nonlinearities come from thermoelectroelastic effects³⁵ and coupling to ensembles of Two Level Systems (TLS), etc. TLS effects are present in many physical systems operating at milli-Kelvin temperatures, such as superconducting qubits, resonators and amplifiers³⁶⁻³⁸, dielectric resonators³⁹, mechanical resonators⁴⁰. Particularly in BAW cavities, the presence of TLSs has been demonstrated through a number of effects, namely, nonlinear losses²⁰, magnetic field sensitivity (hysteresis and memory behavior)⁴⁰ and non-Duffing nonlinearities in devices with high levels of impurities⁴¹, which become dominant at higher frequencies. Thus, to exhibit only by the Duffing nonlinearity, we limit the experiment to low order overtones. Particularly, the third overtone of the fast shear mode (also known as the B-mode) at the frequency $f_c = 5.506033\text{MHz}$ is used to demonstrate the effect.

The experimental setup used in this work is shown in Fig. 1 (A). The BAW cavity is placed inside a copper holder attached to a base plate of a dilution refrigerator cooled to 20mK. The internal volume of the holder is 22mm in diameter (with 1mm groove to hold the quartz plate) and 10mm high. The holder is designed to have its lowest frequency microwave resonances above a few GHz to avoid any coupling to any BAW acoustic modes (lim-

^{a)}Electronic mail: maxim.goryachev@uwa.edu.au

ited to hundreds of MHz). The holder is not hermetically sealed, thus the device is subject to the vacuum level of the dilution refrigerator, which is about 3×10^{-6} mbar. The acoustic modes are excited and read out piezoelectrically using two specially designed coaxial probes coupled to the electric field of the structure. L-shaped and disk-shaped antennas are attached to the central conductor of the co-axial cable protruding from the outer coating by few millimetres and are banded as shown in Fig. 1 (B). This is different from the traditional way of excitation of such devices where one uses relatively large flat electrodes creating an effective coupling capacitor. The probes are positioned to point directly at the centre of the BAW crystal. The geometry of the antennas is optimised to increase the transmission signal. The device is excited using a single-tone RF signal synthesiser locked to a Hydrogen maser to achieve the best frequency stability. The power of the incident signal is controlled via a chain of room temperature attenuators. Low frequency components of the excitation signal are removed with a chain of cold DC blocks with a cut off frequency of a few kHz. The transmitted signal is amplified with a low noise amplifier and detected using an FFT (signal) Analyser.

III. COMB OBSERVATION

In the first experiment, the system response in terms of signal Power Spectral Density (PSD) $S(f)$ is measured as a function of the pump frequency f_p in the vicinity of the acoustic resonance f_s for the constant signal power P . The result is presented in Fig. 2 where each vertical slice of subplot (A) shows a single PSD trace of the output signal for a constant incident signal frequency f_p . Note that each PSD is taken independently for a large number of averages with sufficient time delay between two consecutive measurements. The measurement setup is stable on these time scales because it is locked to an atomic frequency standard. The BAW device parameters are not sensitive to possible temperature fluctuations and other effects. This method ensures the static picture of the response. Fig. 2 demonstrates a frequency comb when the pump signal frequency approaches that of the resonance. The comb shows two thresholds on each side of the resonance. The repetition rate of the comb is about 0.8Hz for $f_p = f_c$, slightly increasing with the pump frequency.

The same threshold in comb generation is observed by varying the incident power for the fixed excitation frequency $f_p \approx f_c$, which is shown in Fig. 3. The figure also demonstrates a decrease of the repetition rate with power.

In addition to the PSD of the transmitted signal, one may measure transmission directly in terms of scattering parameters S_{21} . For this the signal source and the FFT analyzer are replaced with a network analyzer. For this kind of measurement, one sweeps the frequency of the pump signal and measures the ratio of the transmitted and incident wave. To avoid any distortion due to

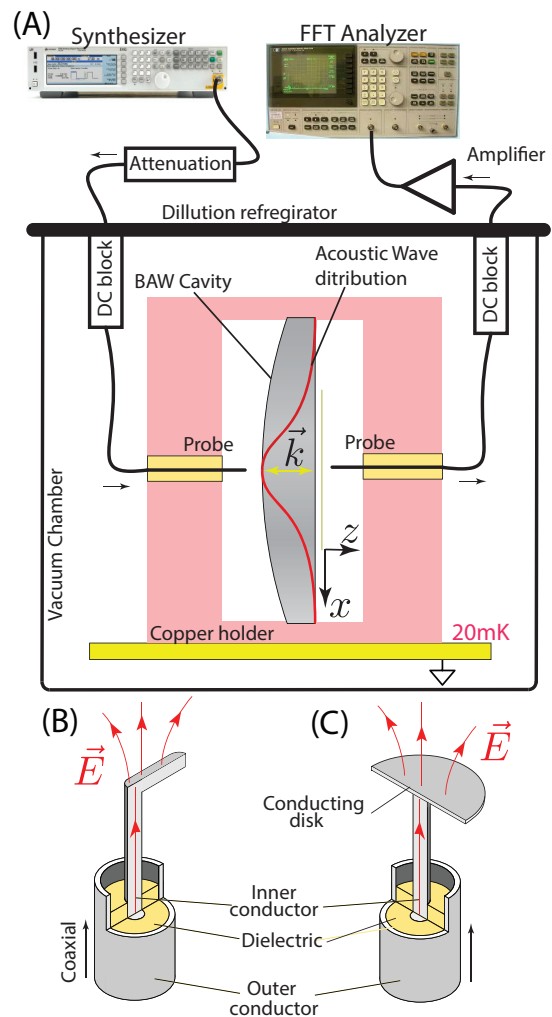


FIG. 1. (A) Experimental setup for excitation of the acoustic frequency comb: a BAW cavity sits vertically in a Copper holder at 20mK in a vacuum chamber. The signal is supplied from the room temperature synthesizer via microwave cables thermalised with DC blocks. The transmitted signal is amplified and analysed with an FFT machine. \vec{k} is the direction of the BAW propagation whose energy has a Gaussian distribution in the crystal plane (red curve). (B) L-shaped excitation antenna (probe) coupling to electric field \vec{E} . (C) Excitation antenna with a disk.

ringing effect, the sweep time for one trace is taken to be 30 minutes. The result is shown in Fig. 7, where for low incident power a classical Duffing behaviour is observed. After a bifurcation, the system demonstrates irregular behavior that corresponds to the comb generation regime. In this area between two 'Threshold' labels, the output signal has more than one frequency component; thus, the transmission as revealed by a receiving detector becomes modulated resulting in this artefact. From these measurements, in the linear regime, the Quality factor of the resonance is estimated as 4.2×10^8 . Fig. 7 also demonstrates the importance of the Duffing nonlinear-

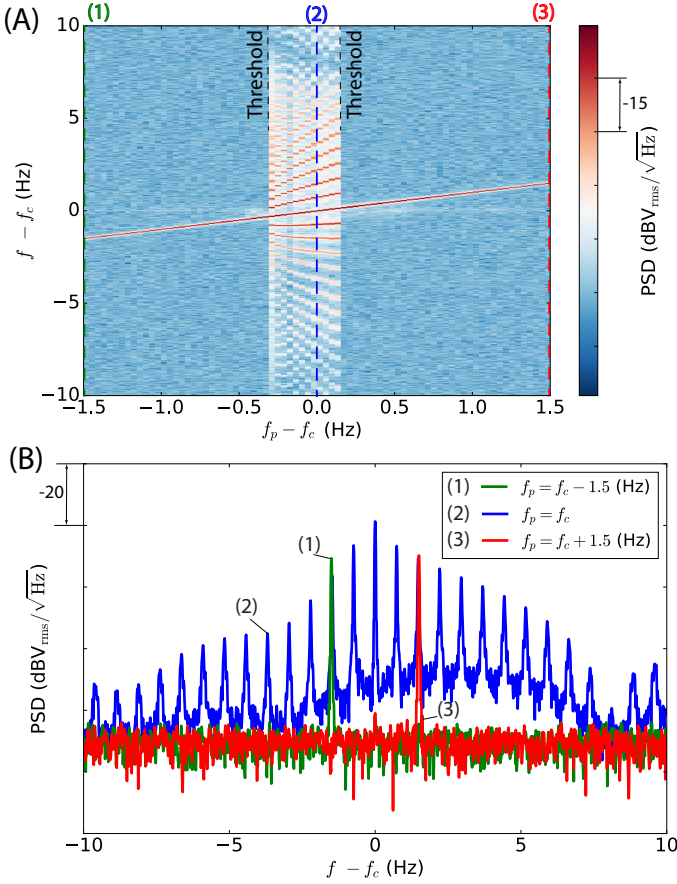


FIG. 2. (A) Output signal PSD $S(f - f_c)$ as a function of pump frequency detuning $f_p - f_c$ for a constant incident power $P = -66$ dBm. (B) Three PSDs for different constant incident frequencies f_p and the same power P corresponding to slices of (A) along the y axis.

ity below the generation threshold that can be seen even for the lowest excitation power. This observation draws an analogy with the photonic frequency comb based on Kerr nonlinearity (due to the third-order $\chi^{(3)}$ component of the electric susceptibility)¹¹, which is a photonic analogue of the phononic Duffing nonlinearity. In both systems, the ultra-low generation threshold is achieved by a combination of nonlinear effects in a low loss environment.

IV. COMB SIMULATION

To understand the comb generation effects in the given acoustic system, one may draw certain analogies and point out some differences with the optical counterparts. Based on the nonlinear elastic equations for a phonon trapping cavity (see Appendix A), one may deduce an equation of motion for a complex envelope of the displacement signal $U_x(z)$ (displacement along in-plane co-

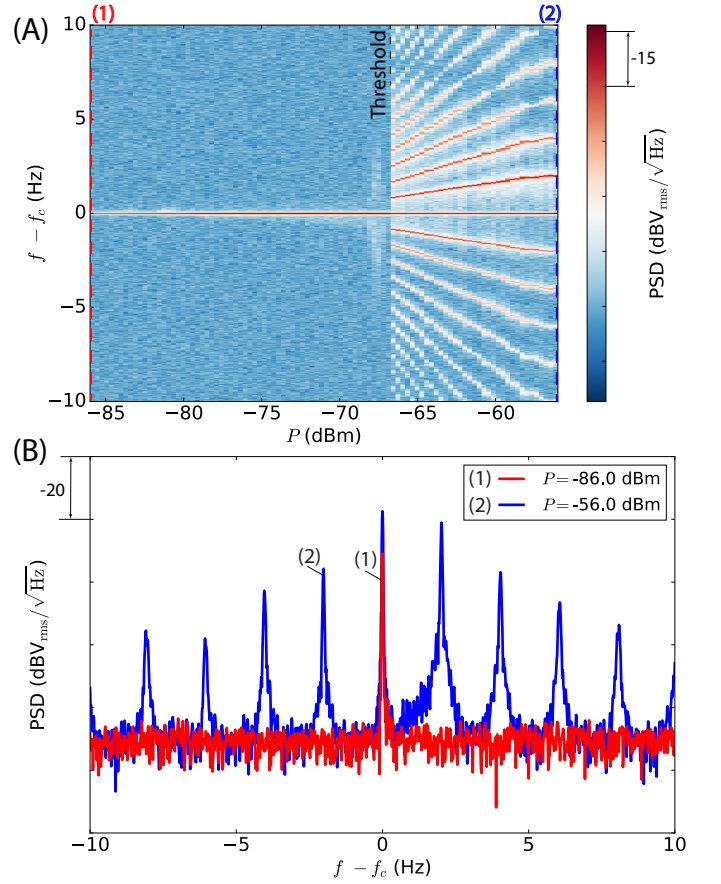


FIG. 3. (A) Output signal PSD $S(f - f_c)$ as a function of pump signal power P for a constant incident frequency $f_p \approx f_c$. (B) Two PSDs for different constant incident frequency f_p and different power levels P corresponding to slices of (A) along the y axis.

ordinate x propagating along the thickness coordinate z):

$$\partial_\tau U_x = -(\kappa + i\Omega)U_x - i\alpha \partial_z^2 U_x - i\gamma \partial_z \left[|\partial_z U_x|^2 \partial_z U_x \right] + F. \quad (1)$$

Here Ω is a scaled resonance frequency, κ is a loss coefficient, F is a complex amplitude of external excitation, and α and γ are frequency scaled stiffness and nonlinear coefficients. The right-hand side of this equation consists of the following terms: resonance frequency (complex and real parts, i.e. damping and central frequency), dispersion term, nonlinear Duffing term and external forcing. This equation is almost identical to the LugiatoLefever equation^{1,42,43}, which captures dynamics of the Kerr frequency combs in optical systems. The major difference is in the nonlinear terms, Kerr and Duffing, where one is given as a function of the complex envelope and the other is given in terms of its first space derivative.

The major difference between optical Kerr combs and

the presented acoustic is the absence of a free spectral range corresponding to the comb signal spacing. In principle, absence of the equally spaced mode structure is also a feature of combs in other mechanical systems¹⁴ and in Whispering Gallery Mode crystals^{9,44}. In the latter case, an extra half degree of freedom arises due to the Fano resonance, the phenomenon which in the BAW community is known as anti-resonance⁴⁵. This typical additional spectral structure is formed by the electrodes spurious capacitance and acoustic equivalent inductance.

To understand the relationship between two types of resonances in the system, we consider a simplified model of a Bulk Acoustic Cavity with additional parasitic capacitance. Such capacitance arises due to excitation electrodes in all types of BAW devices. For an external signal it is composed of parasitic bypass short-circuiting mechanical resonances. To capture the effect of this capacitance and demonstrate how it leads to two mode dynamics of the system, we employ the well known Butterworth-van Dyke model of a BAW device shown in Fig. 4. In this model, mechanical motion of the system is modelled using motional capacitance C_x , inductance L_x and loss resistance R_x . The shunt capacitance is represented by C_0 . The system is coupled to the signal source V_i with loss element R_i and the sink R_s . This is the simplest model of the BAW cavity which does not capture all effects but could be used to demonstrate generation of a photonic comb.

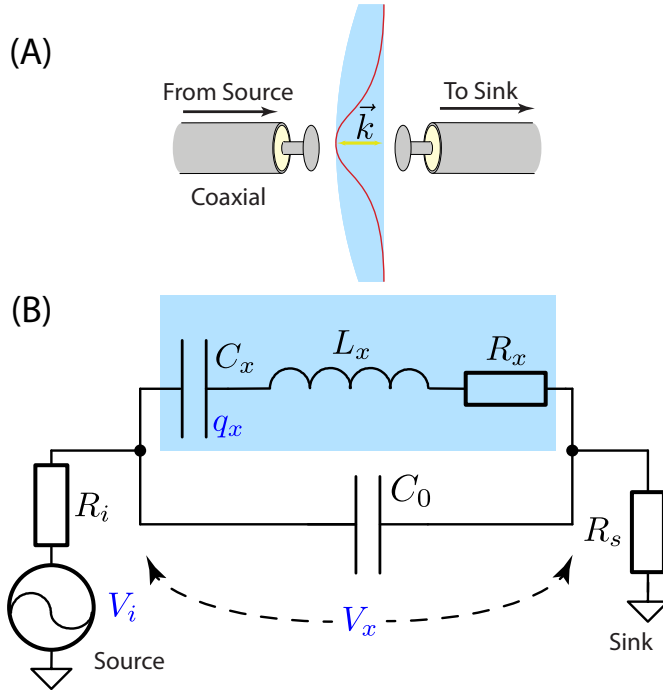


FIG. 4. (A) BAW cavity coupled to input and output transmission lines via disk probes. (B) Equivalent circuit of such device. The blue block represents the pure mechanical degree of freedom.

The linear model in Fig. 4 (B) is described by the following set of differential equations:

$$\begin{aligned} L_x \ddot{q}_x + R_x \dot{q}_x + C_x^{-1} q_x &= V_x, \\ (R_s + R_i)(\dot{q}_0 + \dot{q}_x) + V_x &= V_i, \\ q_0 &= C_0 V_x, \end{aligned} \quad (2)$$

where q_x is a charge on equivalent mechanical capacitor, q_0 is a charge on shunt capacitor and V_x is a voltage across the device. Equivalently, the system may be described as follows:

$$\frac{d}{d\tau} \begin{pmatrix} q_x \\ i_x \\ v_x \end{pmatrix} = \begin{bmatrix} 0 & 1 & 0 \\ -\omega_0^2 & -\gamma_i & g \\ 0 & -g & -\gamma_v \end{bmatrix} \begin{pmatrix} q_x \\ i_x \\ v_x \end{pmatrix} + \begin{pmatrix} 0 \\ 0 \\ f \end{pmatrix} \quad (3)$$

where $\gamma_i = R_x/L_x$, $\gamma_v = 1/(R_i + R_s)/C_0$, $\omega_0^2 = 1/(C_x L_x)$, $g^2 = 1/(C_0 L_x)$, $v_x = V_x/(g L_x)$ and $f_i = V_i \gamma_i / (L_x g)$.

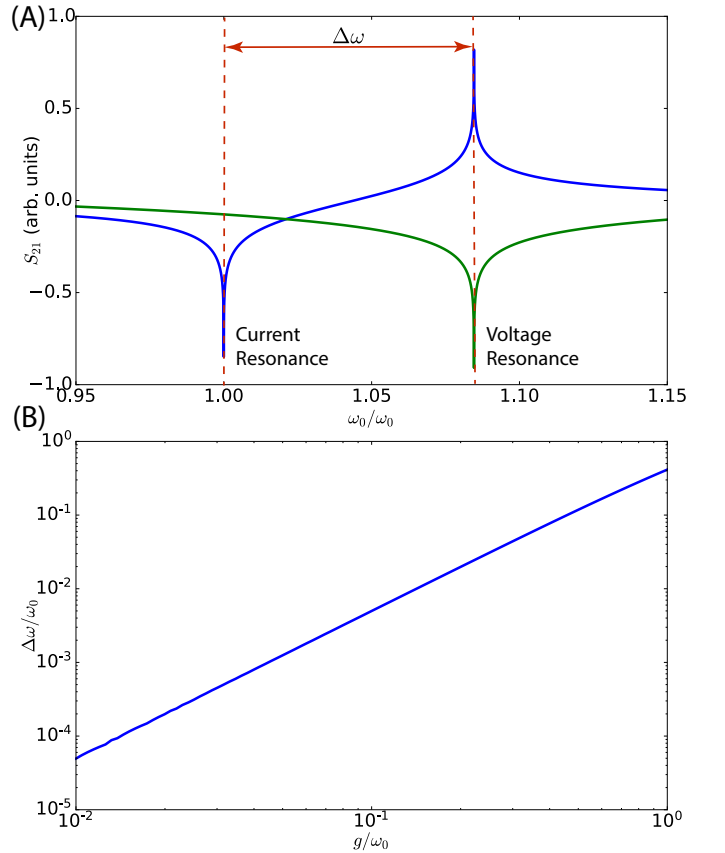


FIG. 5. (A) System response in current and voltage configurations. (B) Scaled frequency difference between current and voltage resonances of $\Delta\omega$ as a function of coupling $g/\omega_0 = \sqrt{C_x/C_0}$.

Resonance of the system (3) can be understood as an equivalent voltage resonance or antiresonance: one imposes voltage v_i over the plate and detect the current i_x .

It corresponds to poles of the 3×3 matrix on the left-hand side of this system. The other type of resonance is an equivalent current corresponding to the situation when one injects current and detects voltage. This situation corresponds to zeros of the 3×3 matrix on the left hand side. The frequency difference between the two increases with increasing shunt capacitance. This is demonstrated in Fig. 5 where the frequency difference between zeros and poles of the system is shown as a function of parameter $g/\omega_0 = \sqrt{C_x/C_0}$. In fact, this parameter can be very small due to smallness of equivalent motional capacitance C_x . This can render the frequency difference to a few Hz. Moreover, the system can be understood as a strongly coupled resonance-antiresonance system where equivalent voltages and currents are mixed through the strong Duffing nonlinearity. This model also explains change of the comb spacing with the applied power by the fact that the resonance frequency shifts with respect to the anti-resonance according to the Duffing model.

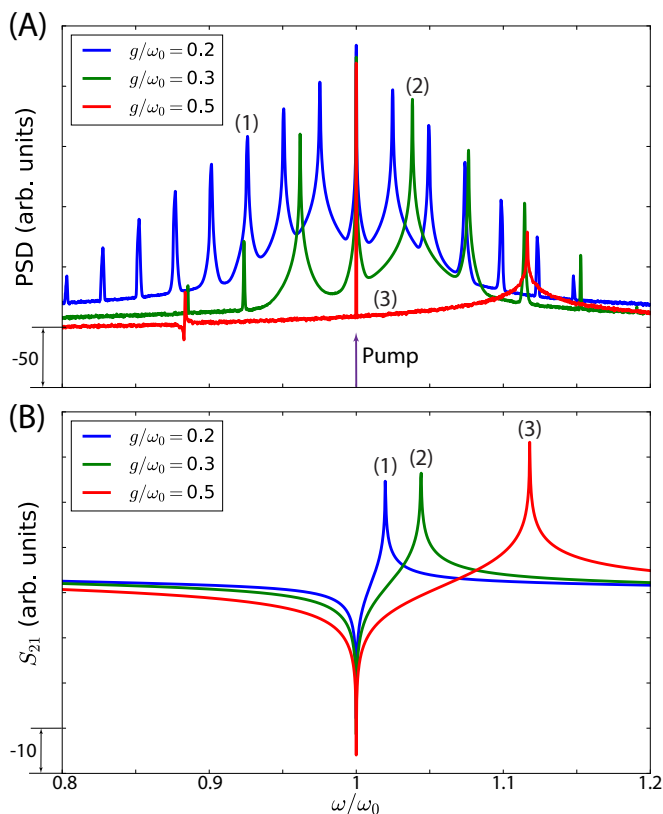


FIG. 6. (A) Power Spectral Density of a steady state signal i_x obtained by numerical simulation of the BAW model with shunt capacitance g/ω_0 and Duffing nonlinearity. (B) Corresponding transmission responses.

To demonstrate the ability of the system to generate a comb, we add a Duffing term κq_x^3 into the second equation of motion in system (3) and simulate the resulting system of nonlinear equations. The simulation is done in the time domain, Power Spectral Densities (PSDs) are

calculated for steady state regimes. Stability of the solutions is verified by changing time steps and tolerances of the simulations. The two loss rates are chosen to be much less than g , i.e. $\gamma_i = 10^{-6}\omega_0$ and $\gamma_i = 10^{-4}\omega_0$. An external signal is pumped at frequency ω_0 . Note should be taken that all simulation parameters are chosen for demonstration purposes and only roughly correspond to the parameters of the actual system. The resulting PSDs for different values of scaled coupling g/ω_0 are presented in Fig. 6 (A). In this Figure, the comb repetition rate is clearly linked to the spacing between resonance and antiresonance in Fig. 6 (B), and affirms the experimental results presented in this work.

V. EFFECT OF ELECTRODES

It has to be emphasised that the comb generation cannot be related to spurious mode coupling. The mode spectrum of the quartz BAW resonators of this kind is well known both from theoretical calculations²⁹ and from experiment, e.g. X-ray topography⁴⁶. The closest modes of the same family with a different in-plane mode numbers are situated at least several kHz away, which comprises a few tens of thousands linewidths. The shear mode with orthogonal polarisation is below 5 MHz. Also, similar comb effects are observed for other shear modes as well. Although the observed generation threshold is higher due to lower Quality factors of the corresponding modes. The longitudinal modes exhibit higher resonance frequencies due to a significantly different wave velocity lacking the comb generation. This may be attributed to the fact that these modes exhibit a very different type of nonlinearity^{20,40}.

As suggested above, the observed comb generation is related to the anti-resonance phenomenon, and thus, on the system response should significantly depends on the geometry of the excitation electrodes. To verify this statement the system has been excited with a different type of antenna. In the previous results, the system was excited using L-shaped asymmetric probes. A qualitatively different result is observed when both probe antennas have a metallic disk (1cm diameter sticking 4mm from the copper surface) at their end which is shown in Fig. 1 (B). The system response for such configuration is shown in Fig. 8. Here, the comb appear to be at lower incident power level (-80dBm) with clear one-sided character. The comb repetition rate is about 1.5 Hz and can be adjusted in the range between 0.7 and 2 Hz. Due to very low level of the output signal, these results do not display a sharp threshold as it occurs below the noise floor. Another interesting phenomenon shown in this figure is the increase of noise in the generation regime (curve (2)). Such excess noise in BAW devices and its dependence on power levels have been a subject of investigation for many decades as it limits the performance of these devices at room temperature^{47,48}. Although the origins of such phenomena are still unknown.

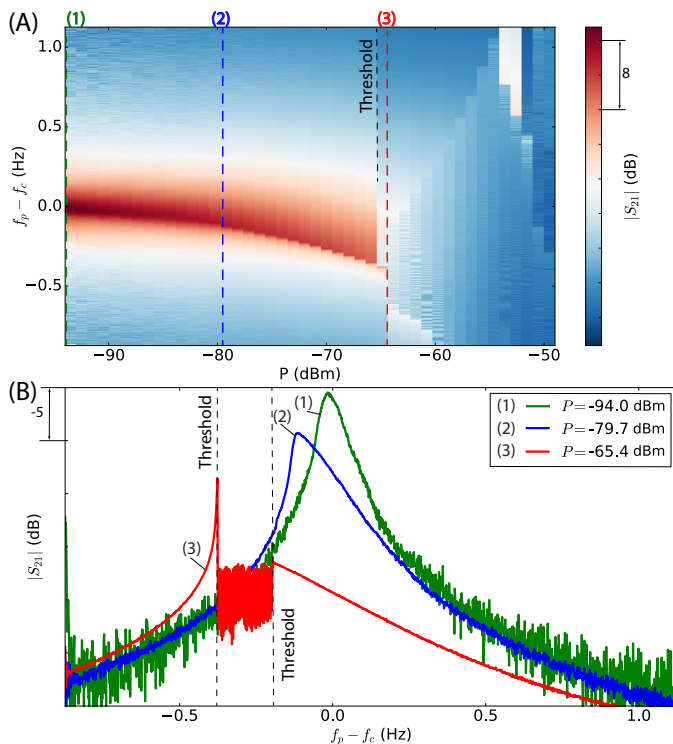


FIG. 7. (A) Transmission through the BAW cavity $|S_{21}(f - f_c)|$ for different values of the incident power P . (B) Three examples of transmission for different constant power levels corresponding to slices of (A) along the y axis.

VI. CONCLUSION

In summary, we experimentally demonstrated excitation of ultra-low threshold phononic frequency combs in a cryogenic environment. The result is achieved at very low acoustic loss and strong nonlinearities. The comb generation is supported by the anti-resonance phenomenon due to electrodes that is demonstrated by numerical simulation. The comb profile could be engineered with the electrode geometry. On the other hand the method does not require special designs of mode spectra or external microwave or optical signals. The system demonstrates similarities with optical Kerr effect frequency comb generators based on optical microresonators. Because of its ultra low power, the system becomes compatible with quantum hybrid systems^{17–19}, particularly superconducting and impurity defects qubits, and can be used for their manipulation^{49,50}. Other applications include sensors, phonon based computations⁵¹ and tests of fundamental physics tests^{20–23}. Finally, such systems may be used to improve the BAW device technology through deeper understanding of fundamental processes in solid state acoustics and limiting mechanisms such as the drive level sensitivity and excess noise^{47,48}.

This work was supported by the Australian Research Council Grant No. CE170100009.

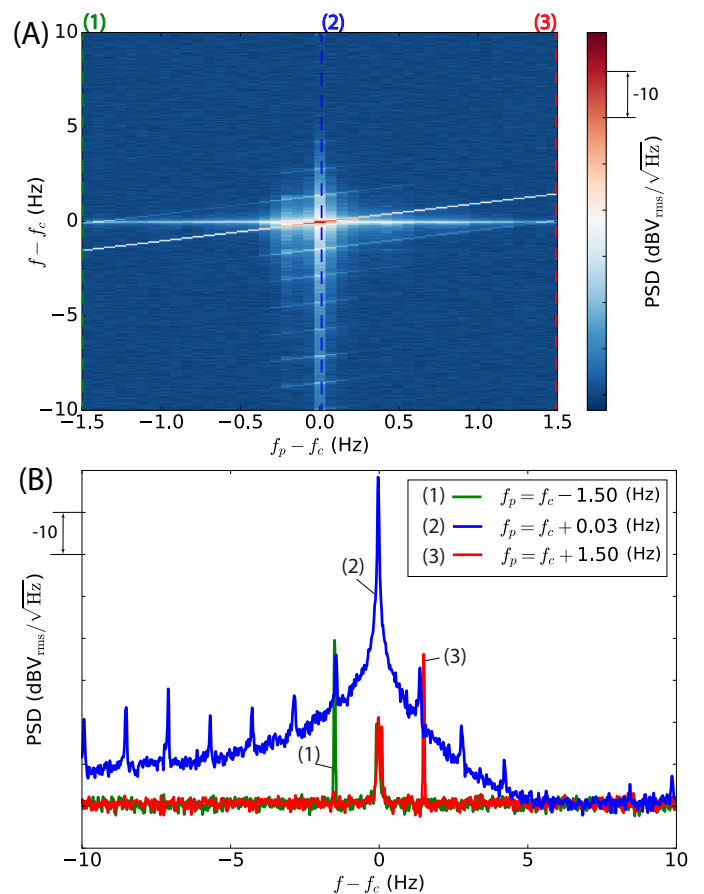


FIG. 8. (A) Output signal PSD $S(f - f_c)$ as a function of pump frequency detuning $f_p - f_c$ for a constant incident power $P = -80$ dBm for a system excited with a metallic disk antennas. (B) Three PSDs for different constant incident frequency f_p and the same power P corresponding to slices of (A) along y axis.

REFERENCES

- ¹Y. Chembo, *Nanophotonics* **5**, 214 (2016).
- ²L.-S. Ma, Z. Bi, A. Bartels, L. Robertsson, M. Zucco, R. S. Windeler, G. Wilpers, C. Oates, L. Hollberg, and S. A. Diddams, *Science* **303**, 1843 (2004).
- ³R. Holzwarth, M. Zimmermann, T. Udem, and T. W. Hansch, *IEEE Journal of Quantum Electronics*, *IEEE Journal of Quantum Electronics* **37**, 1493 (2001).
- ⁴J. Milló, M. Abgrall, M. Lours, E. M. L. English, H. Jiang, J. Guéna, A. Clairon, M. E. Tobar, S. Bize, Y. Le Coq, and G. Santarelli, *Applied Physics Letters* **94**, 141105 (2009).
- ⁵N. Picqué and T. W. Hänsch, *Nature Photonics* **13**, 146 (2019).
- ⁶M. C. Stowe, M. J. Thorpe, A. Pe'er, J. Ye, J. E. Stalnaker, V. Gerginov, S. A. Diddams, E. Arimondo, P. R. Berman, and C. C. Lin, “Direct frequency comb spectroscopy,” in *Advances In Atomic, Molecular, and Optical Physics*, Vol. 55 (Academic Press, 2008) pp. 1–60.
- ⁷F. Adler, K. Moutzouris, A. Leitenstorfer, H. Schnatz, B. Lipphardt, G. Grosche, and F. Tauser, *Optics Express*, *Optics Express* **12**, 5872 (2004).
- ⁸G. A. Sefer and K. . Kitayama, *Journal of Lightwave Technology*, *Journal of Lightwave Technology* **16**, 1596 (1998).

- ⁹D. L. Creedon, K. Benmessai, and M. E. Tobar, *Phys. Rev. Lett.* **109**, 143902 (2012).
- ¹⁰A. Pasquazi, M. Peccianti, L. Razzari, D. J. Moss, S. Coen, M. Erkintalo, Y. K. Chembo, T. Hansson, S. Wabnitz, P. Del'Haye, X. Xue, A. M. Weiner, and R. Morandotti, *Microcombs: A novel generation of optical sources*, *Physics Reports* **729**, 1 (2018).
- ¹¹P. Del'Haye, A. Schliesser, O. Arcizet, T. Wilken, R. Holzwarth, and T. J. Kippenberg, *Nature* **450**, 1214 EP (2007).
- ¹²I. S. Maksymov and A. D. Greentree, *Nanophotonics* **8**, 367 (2019).
- ¹³L. S. Cao, D. X. Qi, R. W. Peng, M. Wang, and P. Schmelcher, *Physical Review Letters* **112**, 075505 (2014).
- ¹⁴A. Ganesan, C. Do, and A. Seshia, *Physical Review Letters* **118**, 033903 (2017).
- ¹⁵M. Hase, M. Katsuragawa, A. Monia Constantinescu, and H. Pektel, *EPJ Web of Conferences* **41**, 04020 (2013).
- ¹⁶P. Salzenstein, A. Kuna, L. Sojdr, and J. Chauvin, *Electronics Letters* **46**, 1433 (October 2010).
- ¹⁷Y. Chu, P. Kharel, W. H. Renninger, L. D. Burkhart, L. Frunzio, P. T. Rakich, and R. J. Schoelkopf, *Science* **358**, 199 (2017).
- ¹⁸P. Kharel, Y. Chu, M. Power, W. H. Renninger, R. J. Schoelkopf, and P. T. Rakich, *APL Photonics* **3**, 066101 (2018).
- ¹⁹S. Kotler, R. W. Simmonds, D. Leibfried, and D. J. Wineland, *Physical Review A* **95**, 022327 (2017).
- ²⁰M. Goryachev and M. E. Tobar, *Physical Review D* **90**, 102005 (2014).
- ²¹S. Singh, L. A. D. Lorenzo, I. Pikovski, and K. C. Schwab, *New Journal of Physics* **19**, 073023 (2017).
- ²²A. Lo, P. Haslinger, E. Mizrachi, L. Anderegg, H. Müller, M. Hohensee, M. Goryachev, and M. E. Tobar, *Phys. Rev. X* **6**, 011018 (2016).
- ²³P. Bushev, J. Bourhill, M. Goryachev, N. Kukharchyk, E. Ivanov, S. Galliou, M. Tobar, and S. Danilishin, *arxiv.org quant-ph*, 1903.03346 (2019).
- ²⁴E. P. C. Lai, B. L. Chan, and S. Chen, *Applied Spectroscopy*, *Applied Spectroscopy* **42**, 526 (1988).
- ²⁵A. W. Czanderna, C. Lu, C. LU, and A. W. CZANDERNA, "Chapter 1 - introduction, history, and overview of applications of piezoelectric quartz crystal microbalances," in *Methods and Phenomena*, Vol. 7 (Elsevier, 1984) pp. 1–18.
- ²⁶R. Fogel, J. Limson, and A. A. Seshia, *Essays In Biochemistry* **60**, 101 (2016).
- ²⁷D. Johannsmann, *Physical Chemistry Chemical Physics* **10**, 4516 (2008).
- ²⁸T. F. Roque, F. Marquardt, and O. M. Yevtushenko, *arxiv* **1909.03126** (2019).
- ²⁹D. S. Stevens and H. F. Tiersten, *The Journal of the Acoustical Society of America*, *The Journal of the Acoustical Society of America* **79**, 1811 (1986).
- ³⁰J. A. Kusters, 1981 Ultrasonics Symposium , 402 (14-16 Oct. 1981).
- ³¹S. Galliou, M. Goryachev, R. Bourquin, P. Abbe, J. Aubry, and M. Tobar, *Scientific Reports* **3** (2013).
- ³²J. Gagnepain and R. Besson, "Physical acoustics," (Elsevier, 2012) Chap. Nonlinear Effects in Piezoelectric Quartz Crystals, pp. 245–288.
- ³³H. Tiersten, *J. Acoust. Soc. Am.* **59**, 866 (1976).
- ³⁴J. Nosek, *IEEE Transactions on Ultrasonics, Ferroelectrics and Frequency Control* **46**, 823 (1999).
- ³⁵H. Tiersten, *Inr. J. Engng Sci.* **9**, 587 (1971).
- ³⁶J. Lisenfeld, G. J. Grabovskij, C. Müller, J. H. Cole, G. Weiss, and A. V. Ustinov, *Nature Communications* **6**, 6182 EP (2015).
- ³⁷J. Burnett, L. Faoro, I. Wisby, V. L. Gurtovoi, A. V. Chernykh, G. M. Mikhailov, V. A. Tulin, R. Shaikhaidarov, V. Antonov, P. J. Meeson, A. Y. Tzalenchuk, and T. Lindström, *Nature Communications* **5**, 4119 EP (2014).
- ³⁸S. M. Anton, J. S. Birenbaum, S. R. O'Kelley, V. Bolkhovskiy, D. A. Braje, G. Fitch, M. Neeley, G. C. Hilton, H. M. Cho, K. D. Irwin, F. C. Wellstood, W. D. Oliver, A. Shnirman, and J. Clarke, *Physical Review Letters* **110**, 147002 (2013).
- ³⁹D. L. Creedon, Y. Reshitnyk, W. Farr, J. M. Martinis, T. L. Duty, and M. E. Tobar, *Applied Physics Letters* **98**, 222903 (2011).
- ⁴⁰M. Goryachev, S. Galliou, and M. E. Tobar, *Physical Review B* **100**, 174108 (2019).
- ⁴¹M. Goryachev, W. Farr, E. Ivanov, and M. Tobar, *Journal of Applied Physics* **114**, 094506 (2013).
- ⁴²L. A. Lugiato and R. Lefever, *Physical Review Letters* **58**, 2209 (1987).
- ⁴³F. Castelli, M. Brambilla, A. Gatti, F. Prati, and L. A. Lugiato, *The European Physical Journal D* **71**, 84 (2017).
- ⁴⁴N. R. Nand, M. Goryachev, J.-M. I. Floch, D. L. Creedon, and M. E. Tobar, *Journal of Applied Physics*, *Journal of Applied Physics* **116**, 134105 (2014).
- ⁴⁵J. Vig, *Quartz Crystal Resonators and Oscillators For Frequency Control and Timing Applications - A Tutorial*, US Army Communications-Electronics Research, Development & Engineering Center (2008).
- ⁴⁶D. V. Irzhak, D. V. Roshchupkin, D. V. Punegov, and S. A. Sakharov, *Bulletin of the Russian Academy of Sciences: Physics* **71**, 72 (2007).
- ⁴⁷J. J. Gagnepain, M. Oliver, and F. L. Walls, *37th Annual Symposium on Frequency Control. 1983*, 37th Annual Symposium on Frequency Control. 1983 , 218 (1983).
- ⁴⁸R. Boudot, G. Martin, J.-M. Friedt, and E. Rubiola, *Journal of Applied Physics*, *Journal of Applied Physics* **120**, 224903 (2016).
- ⁴⁹C. Hann, C.-L. Zou, Y. Zhang, Y. Chu, R. Schoelkopf, S. Girvin, and L. Jiang, *arXiv arXiv:1906.11340v1* (2019).
- ⁵⁰H. Chen, N. F. Opondo, B. Jiang, E. R. MacQuarrie, R. S. Davneau, S. A. Bhave, and G. D. Fuchs, *Nano Letters*, *Nano Letters* **19**, 7021 (2019).
- ⁵¹S. N. R. Kazmi, M. A. A. Hafiz, K. N. Chappanda, S. Ilyas, J. Holguin, P. M. F. J. Costa, and M. I. Younis, *Nanoscale* **9**, 3449 (2017).
- ⁵²H. Tiersten and D. Stevens, *J. Acoust. Soc. Am.* **80**, 1122 (1986).
- ⁵³H. Tiersten, *J. Acoust. Soc. Am.* **57**, 667 (1975).

Appendix A: Elastic Nonlinearity in a BAW Cavity

To discuss nonlinearities in a curved (phonon trapping) BAW cavity, we consider a crystal plate oriented in such a way that the the crystal thickness is along coordinate z (see Fig. 1). Nonlinear Equations of Motion (EOM) for mechanical displacement $\mathbf{u} = (u_x, u_y, u_z)^T$ of a shear mode with u_x being the major component ($|\partial_z u_i| \gg |\partial_x u_i|, |\partial_y u_i|$) are presented as follows⁵²:

$$\begin{aligned} \rho \partial_t^2 u_x - \bar{c}^{(1)} \partial_z^2 u_x - \tilde{\gamma} \partial_z (\partial_z u_x)^3 - \tilde{\beta}_1 \partial_z (\partial_z u_x)^2 \\ - 2\tilde{\beta}_2 \partial_z (\partial_z u_x \partial_z u_z) - 2\tilde{\beta}_2 \partial_z (\partial_z u_x \partial_z u_y) = f_x, \\ \rho \partial_t^2 u_y - \bar{c}^{(2)} \partial_z^2 u_y - \tilde{\beta}_2 \partial_z (\partial_z u_x)^2 = f_y, \\ \rho \partial_t^2 u_z - \bar{c}^{(3)} \partial_z^2 u_z - \tilde{\beta}_2 \partial_z (\partial_z u_x)^2 = f_z, \end{aligned} \quad (\text{A1})$$

where ρ is the specific mass, $\bar{c}^{(i)}$ are so-called piezoelectrically stiffened eigenvalues, f_i are forcing signals, $\tilde{\gamma}$ and $\tilde{\beta}_i$ are nonlinear coefficients. For these equations, one neglects space derivatives with respect to in plane coordinates x and y as variation along these axes is significantly smaller than along the thickness axis z .

Equations (A1) include two types of nonlinearities: self nonlinearities (third and second order in terms of EOMs)

of the main component of displacement u_x , cross nonlinearities between displacements in different directions (all second order). It is widely accepted that the third order nonlinearities in terms of EOMs are the dominant for solids^{34,47,53}, thus for the first simplest model all β coefficients can be neglected. This leaves only one EOM for the major component $u_x(z)$.

By going into the space of slowly varying (both in space and time) complex amplitude $U_x(\tau, z)$, one can transform these equations into the complex form:

$$\partial_\tau U_x = -(\kappa + i\Omega)U_x - i\alpha\partial_z^2 U_x - i\gamma\partial_z \left[|\partial_z U_x|^2 \partial_z U_x \right] + F, \quad (\text{A2})$$

where Ω is a scaled resonance frequency, κ is the loss coefficient, F is a complex amplitude of external excitation, α and γ are frequency scaled stiffness and nonlinear coefficients. The right-hand side of this equation consists of following terms: resonance frequency (complex and real parts, i.e. damping and central frequencies), dispersion

term, nonlinear Duffing term and external forcing.

Equation (A1) describing spatial and temporal evolution of nonlinear acoustic excitation is analogous to the LugiatoLefever equation⁴² used to describe Kerr frequency combs in optical microresonators^{1,43}:

$$\partial_\tau E = -(\kappa + i\Omega)E - i\alpha\partial_z^2 E - i\gamma|E|^2 E + F, \quad (\text{A3})$$

where E is the complex amplitude of the electrical field. Similar to acoustic equation (A2), the right-hand side of the LugiatoLefever equation consists of resonance frequency (complex and real parts, i.e. damping and central frequencies), dispersion, nonlinear Kerr and external forcing terms.

The major difference between the photonic and phononic nonlinear equations (A3) and (A2) is the nonlinear term where one is written in terms of the complex amplitude E and the other is written in terms of the first spatial derivative of the complex amplitude U . The latter arises due to the fact that the nonlinearity originates from the strain rather than displacement itself.